Zhang, Z., Zhang, W., Zhai, Z., and Chen, Q. 2007. "Evaluation of various turbulence models in predicting airflow and turbulence in enclosed environments by CFD: Part-2: comparison with experimental data from literature," *HVAC&R Research*, 13(6).

Evaluation of Various Turbulence Models in Predicting Airflow and Turbulence in Enclosed Environments by CFD: Part-2: Comparison with Experimental Data from Literature

Zhao Zhang, Student Member ASHRAE
Wei Zhang, Member ASHRAE
Zhiqiang Zhai, Member ASHRAE
Qingyan Chen*, Fellow ASHRAE

Numerous turbulence models have been developed in the past decades, and many of them may be used in predicting airflows and turbuence in enclosed environments. It is important to evaluate the generality and robustness of the turbulence models for various indoor airflow senarios. This study evaluated the performance of eight turbulence models potentially suitable for indoor airflow in terms of accuracy and computing cost. These models cover a wide range of computational fluid dyanmics (CFD) approaches including Reynolds averaged Navier-Stokes (RANS) modeling, hybrid RANS and large eddy simulation (or detached eddy simulation, DES), and large eddy simulation (LES). The RANS turbulence models tested include the indoor zero-equation model, three two-equation models (the RNG k-ε, low Reynolds number k-ε, and SST k-ω models), a three-equation model ($\overline{v^2}-f$ model), and a Reynolds stress model (RSM). The investigation tested these models for representative airflows in enclosed environments, such as force convection and mixed convection in ventilated spaces, natural convection with medium temperature gradient in a tall cavity, and natural convection with large temperature gradient in a model fire room. The predicted air velocity, air temperature, Reynolds stresses, and turbulent heat fluxes by the models were compared against the experimental data from the literature. The study also compared the computing time used by each model for all the cases. The results reveal that LES provides the most detailed flow features while the computing time is much higher than RANS models and the accuracy may not always be the highest. Among the RANS models studied, the RNG k-ε and a modified $\overline{v^2}-f$ model have the best overall performance over four cases studied. Meanwhile, the other models have superior performance only in some particular cases. While each turbulence model has good accuracy in certain flow categories, each flow type favors different turbulence models. Therefore, we summarize both the performance of each partcular model in different flows and the best suited turbulence models for each flow category in the conclusions and recommendations.

INTRODUCTION

The companion paper (Zhai et al., 2007) reviewed the recent development and applications of computational fluid dynamics (CFD) approaches and turbulence models for predicting air motion in enclosed spaces. The review identified eight prevalent and/or recently proposed turbulence models for indoor airflow prediction. These models include: the indoor zero-equation model (0-eq.) by Chen and Xu (1998), the RNG k-ε model by Yakhot and Orszag (1986), a low Reynolds number k-ε model (LRN-LS) by Launder and Sharma (1974), the SST k-ω model (SST) by Menter (1994), a modified v2f model (v2f-dav) by Davidson et al. (2003), a Reynolds

* **Zhao Zhang** is a PhD candidate, **Wei Zhang** is an affiliate, and **Qingyan Chen** is a professor in the School of Mechanical Engineering, Purdue University, West Lafayette, IN. **Zhiqiang Zhai** is an assistant professor in the Department of Civil, Environmental & Architectural Engineering, University of Colorado, Boulder, CO.

stress model (RSM-IP) by Gibson and Launder (1978), the large eddy simulation (LES) with a dynamic subgrid scale model (LES-Dyn) (Germano et al. 1991 and Lilly 1992), and the detached eddy simulation (DES-SA) by Shur et al. (1999). This paper evaluates and compares the selected turbulence models for several indoor benchmark cases that represent the primary flow mechanism of air movement in enclosed environments.

All these turbulence model equations mentioned above can be written in a general form as:

$$\rho\frac{\partial\bar{\phi}}{\partial t}+\rho\overline{u}_j\frac{\partial\bar{\phi}}{\partial x_j}-\frac{\partial}{\partial x_j}\left[\Gamma_{\phi,\mathrm{eff}}\frac{\partial\bar{\phi}}{\partial x_j}\right]=S_\phi \qquad (1)$$

where ϕ represents variables, $\Gamma_{\phi,\mathrm{eff}}$ the effective diffusion coefficient, and S_ϕ the source term of an equation. Table 1 briefly summarizes the mathematical expressions of the eight turbulence models selected. In Table 1, u_i is the velocity component in i direction, T the air temperature, k the kinetic energy of turbulence, ε the dissipation rate of turbulent kinetic energy, and ω the specific dissipation rate of turbulent kinetic energy. P the air pressure, H the air enthalpy, μ_t the eddy viscosity, G_ϕ the turbulence production for ϕ, and S the rate of the strain. The other coefficients are case-specific and only some important ones are introduced here.

For the 0-eq. model, V is the velocity magnitude and *l* is the wall distance. The G_B is the buoyancy production term for the RNG k-ε model. For LRN-LS model; the f_μ, $C^*_{\varepsilon 1}$, $C^*_{\varepsilon 2}$ are the three modified coefficients (i.e., damping functions) to the standard k-ε model; and D and E are two additional terms. These five major modifications in the LRN model are responsible for improving model performance near the wall. In SST model the Y is the dissipation term in the k and ω equations. The F_1 and F_2 are blending functions that control the switch between the transformed k- ε model and the standard k-ω model. The D_ω is produced from the transformed k-ε model. So it vanishes in the k-ω mode when the blending function F_1 is unit. In v2f-dav model (Davidson et al., 2003), the $\overline{v'^2}$ is the fluctuating velocity normal to the nearest wall. The *f* is part of the $\overline{v'^2}$ source term that accounts for non-local blocking of the wall normal stress. The *f* is implicitly expressed by an elliptical partial differential equation. So the scalar *f* can be in principle solved by the same partial-differential-equation solver as for the other variables. Note that the T in v2f-dav model also represents the turbulence time scale. In RSM model, the ϕ_{lm} is the pressure strain term and requires further modeling. In the present study, a liner pressure strain model by Gibson and Launder (1978) is used.

In the LES, the over bar represents the filtering. The τ^S_{ij} and h^S_j represent the subgrid scale (SGS) stress and heat flux. Lilly's SGS model (1992) adopts the Boussinesq hypothesis and derives methods to calculate the coefficient C_s in the eddy viscosity expression automatically. The presented DES (Shur et al. 1999) couples the LES with a one-equation RANS model (Spalart and Allmaras, 1992). This one-equation model solves directly a modified eddy viscosity rather than the turbulence kinetic energy as most one-equation models do. The d is the wall distance, the f_{v1} and f_{v2} are the damping functions. Due to the space limit of the paper, a more detailed description of these models is not possible. Since many of the models are available in some commercial software, one could also refer to the user manual (e.g., FLUENT, 2005) for detailed model descriptions.

1

Table 1. Coefficients and Source Terms for Eq. (1)

	ϕ	$\Gamma_{\phi,\text{eff}}$	S_ϕ	Constants and coefficients
Reynolds Averaged Navier-Stokes (RANS) methods				
Reynolds filtered variables for (1)-(6)	1 u_i T C	0 $\mu+\mu_t$ $\mu/\sigma_T+\mu_t/\sigma_{T,t}$ $\mu/\sigma_C+\mu_t/\sigma_{C,t}$	$-\partial p/\partial x_i-\rho\beta g_i(H-H_o)/C_p$ S_H S_C	Note : $S_{ij}=\frac{1}{2}\left(\frac{\partial \bar{u}_i}{\partial x_j}+\frac{\partial \bar{u}_j}{\partial x_i}\right)$; $\Omega_{ij}=\frac{1}{2}\left(\frac{\partial \bar{u}_i}{\partial x_j}-\frac{\partial \bar{u}_j}{\partial x_i}\right)$
(1) 0-eq.	–	–	–	$\mu_t=C\rho V l$; $C=0.03874$; $l-\text{wall distance}$
(2) RNG k-ε	k ε	$\mu+\mu_t/\sigma_{k,t}$ $\mu+\mu_t/\sigma_{\varepsilon,t}$	$G_k-\rho\varepsilon+G_B$ $C_{\varepsilon 1}G_k\varepsilon/k-C_{\varepsilon 2}\rho\varepsilon^2/k$	$\mu_t=C_\mu\rho\frac{k^2}{\varepsilon}$; $G_k=\mu_t S^2$; $S\equiv\sqrt{2S_{ij}S_{ij}}$; $G_B=\beta g_i\left(\mu_t/\sigma_{T,t}\right)\frac{\partial \bar{T}}{\partial x_i}$ $C_{\varepsilon 1}$=1.44, $C_{\varepsilon 2}$=1.92, C_μ=0.09, $\sigma_{T,t}$=0.9, $\sigma_{k,t}$=1.0, $\sigma_{\varepsilon,t}$=1.3, $\sigma_{C,t}$=1.0
(3) LRN-LS	k ε	$\mu+\mu_t/\sigma_{k,t}$ $\mu+\mu_t/\sigma_{\varepsilon,t}$	$G_k-\rho\varepsilon+G_B+D$ $C^*_{\varepsilon 1}G_k\varepsilon/k-C^*_{\varepsilon 2}\rho\varepsilon^2/k+E$	$\mu_t=f_\mu C_\mu\rho k^2/\varepsilon$; $f_\mu=\exp\left[-3.4/\left(1+\text{Re}_t/50\right)^2\right]$; $D=2\mu_t\left(\frac{\partial k^{1/2}}{\partial x_\perp}\right)^2$; $E=\frac{2\mu\mu_t}{\rho}\left(\frac{\partial^2 u_{//}}{\partial^2 x_\perp}\right)^2$; $C^*_{\varepsilon 1}=C_{\varepsilon 1}$; $C^*_{\varepsilon 2}=C_{\varepsilon 2}\left[1-0.3\exp\left(-\text{Re}_t^2\right)\right]$
(4) SST k-ω	k ω	$\mu+\mu_t/\sigma_k$ $\mu+\mu_t/\sigma_\omega$	$\tilde{G}_k-Y_k$ $G_\omega-Y_\omega+D_\omega$	$\mu_t=\frac{\rho k}{\omega}\frac{1}{\max\left[1/\alpha^*,SF_2/a_1\omega\right]}$; $\tilde{G}_k=\min\left(G_k,10\rho\beta^*k\omega\right)$; $G_\omega=\frac{\rho\alpha G_k}{\mu_t}$; $Y_k=\rho\beta^*k\omega$; $Y_\omega=\rho\beta\omega^2$; $D_\omega=2\left(1-F_1\right)\rho\sigma_{\omega,2}\frac{1}{\omega}\frac{\partial k}{\partial x_j}\frac{\partial \omega}{\partial x_j}$; $\alpha^*=\frac{\beta_i/3+(\text{Re}_t/6)}{1+(\text{Re}_t/6)}$; $\text{Re}_t=\frac{\rho k}{\mu\omega}$; $\beta^*=\beta^*_\infty\frac{4/15+(\text{Re}_t/8)^4}{1+(\text{Re}_t/8)^4}$;

(5) v2f-dav	k ε $\overline{v'^2}$	$\mu + \mu_t/\sigma_{k,t}$ $\mu + \mu_t/\sigma_{\varepsilon,t}$ $\mu + \mu_t/\sigma_{k,t}$	$G_k - \rho\varepsilon$ $C_{\varepsilon 1}G_k\varepsilon/k - C_{\varepsilon 2}\rho\varepsilon^2/k$ $S_{\overline{v'^2}}$	$f - L^2\nabla^2 f = \frac{C_1}{T}\left(\frac{2}{3} - \frac{\overline{v'^2}}{k}\right) + C_2\frac{G_k}{\rho k} + 5\frac{\overline{v'^2}}{kT}$; $T = \max\left(\frac{k}{\varepsilon}, 6\sqrt{\frac{\mu}{\rho\varepsilon}}\right)$; $L = C_L \max\left[\frac{k^{3/2}}{\varepsilon}, C_\eta\left(\frac{\mu}{\rho}\right)^{3/4}\varepsilon^{-1/4}\right]$; $\mu_t = \rho \min\left\{0.22\overline{v'^2}T, 0.09\frac{k^2}{\varepsilon}\right\}$ $C_{\varepsilon 1}=1.4\left(1+0.05\sqrt{k/\overline{v'^2}}\right)$; $C_{\varepsilon 2}=1.9$, $C_1=1.4$, $C_2=0.3$, $C_\mu=0.22$, $C_L=0.23$, $C_\eta=70$, $\sigma_{k,t}=1.0$, $\sigma_{\varepsilon,t}=1.3$
(6) RSM-IP	$\overline{u_l'u_m'}$	$\mu + \mu_t/\sigma_j$	$P_{lm} + G_{lm} + \phi_{lm} - \varepsilon_{lm}$	$P_{lm} \equiv -\rho\left(\overline{u_l'u_j'}\frac{\partial u_m}{\partial x_j} + \overline{u_m'u_j'}\frac{\partial u_l}{\partial x_j}\right)$; $G_{lm} = -\rho\beta\left(g_l\overline{u_l'T'} + g_m\overline{u_m'T'}\right)$; $\phi_{lm} = \overline{p\left(\frac{\partial u_m'}{\partial x_l} + \frac{\partial u_l'}{\partial x_m}\right)}$; $\varepsilon_{lm} = \frac{2}{3}\delta_{lm}\varepsilon$;
Large Eddy Simulation (LES) (All variables are filtered)				
(7) LES-Dyn	1 u_i T	0 μ μ/σ_T	$-\partial\bar{p}/\partial x_i - \partial\tau_{ij}^S/\partial x_j$ $-\partial h_j^S/\partial x_j$	$\tau_{ij}^S \equiv \overline{u_i u_j} - \bar{u}_i\bar{u}_j$; $h_j^S \equiv \overline{Tu_j} - \bar{T}\bar{u}_j$; $\tau_{ij}^S = \mu_t\left(\frac{\partial\bar{u}_i}{\partial x_j} + \frac{\partial\bar{u}_j}{\partial x_i}\right) + \frac{1}{3}\rho\tau_{kk}^S\delta_{ij}$; $\mu_t = \rho(C_s\Delta)^2\sqrt{2\bar{S}_{ij}\bar{S}_{ij}}$
Detached Eddy Simulation (DES) switches between a RANS (e.g. S-A) and a LES				
(8) DES-SA	$\tilde{\nu}$	$\mu/\sigma_{\tilde{\nu}} + \mu_t/f_{v1}\sigma_{\tilde{\nu}}$	$G_{\tilde{\nu}} - Y_\nu + \frac{C_{b2}\rho}{\sigma_{\tilde{\nu}}}\left(\frac{\partial\tilde{\nu}}{\partial x_j}\right)^2$	$\mu_t = f_{v1}\rho\tilde{\nu}$; $G_{\tilde{\nu}} = C_{b1}\rho\tilde{\nu}\left[\lvert\Omega\rvert + \tilde{\nu}f_{v2}/\left(\kappa^2 d^2\right)\right]$; $Y_\nu = C_{\omega 1}\rho f_\omega\left(\tilde{\nu}/d\right)^2$

1

NUMERICAL METHOD

This study used a commercial CFD software, FLUENT (version 6.2) to conduct all the numerical investigations to be discussed in the next section. Most of the models shown in Table 1 are available in FLUENT except the modified v2f-dav model. We applied user defined scalar (UDS) transport equations and coded user defined functions (UDF) to describe the governing equations of the k, ε, and $\overline{v'^2}$ as well as the elliptical partial differential equation for *f*. The RANS models used the second order upwind scheme for all the variables except pressure. The discretization of pressure is based on a staggered scheme, PRESTO! (FLUENT, 2005). The SIMPLE algorithm was adopted to couple the pressure and momentum equations. If the sum of absolute normalized residuals for all the cells in flow domain became less than 10^{-6} for energy and 10^{-3} for other variables, the solution was considered converged. Grid dependence of each case was checked using two to four different grids to ensure that grid resolution would not have a notable impact on the results.

RESULTS AND ANALYSIS

This study evaluated the performance of the eight selected models by simulating the distributions of airflow, air temperature, and turbulence quantities in four different enclosed environments. The four cases under investigation are natural convection in a tall cavity, forced convection in a model room with partitions, mixed convection in a square cavity, and strong buoyancy flow in a model fire room. The first three cases are benchmark cases that represent the most basic flow features in enclosed environment. The fourth case is more challenging and can be used to test model robustness in the present research. Figure 1 shows the geometric and airflow information of the four cases. Detailed comparison and result analyses are discussed in the following subsections.

Natural Convection in a Tall Cavity

Natural convection in enclosed environment is attributed to the buoyancy effect caused by the existence of gravity and fluid density differential. Typical examples of natural convection in enclosed environment include: thermal plumes generated by heat sources, and airflow near a wall or a window generated by temperature difference between the surface and the air, etc.

Betts and Bokhari (2000) conducted an experimental investigation of natural convection in a tall cavity as shown in Figure 1(a). The dimensions of the cavity were 2.18 m high by 0.076 m wide by 0.52 m deep. The cold and hot walls had uniform temperatures of $15.1\,^{\circ}\mathrm{C}$ and $34.7\,^{\circ}\mathrm{C}$, respectively. The Rayleigh number based on the cavity width was 0.86×10^{6}. The large ratio of cavity height and width ensured that the airflow in the core region was fully turbulent despite of relatively low Rayleigh number. Their experimental data also showed the airflow pattern was approximately two-dimensional in the vicinity of the center plane. The air temperature inside the cavity was measured by a thermocouple. The air velocity was measured by a single component laser-Doppler anemometry (LDA) system.

The numerical results presented were based on a 25×150 non-uniform two dimensional grid for all RANS models except the LRN-LS and a 25×150×50 three dimensional grid for LES and DES. The corresponding y+ was about 0.3 for the first grid close to the walls while the y+ for LRN-LS grid was less than 0.1. Since the calculated y+ is rather small, the enhanced wall treatment (FLUENT, 2005) was adopted for RNG k-ε and RSM-IP models. The same treatment was also adopted in the others cases.

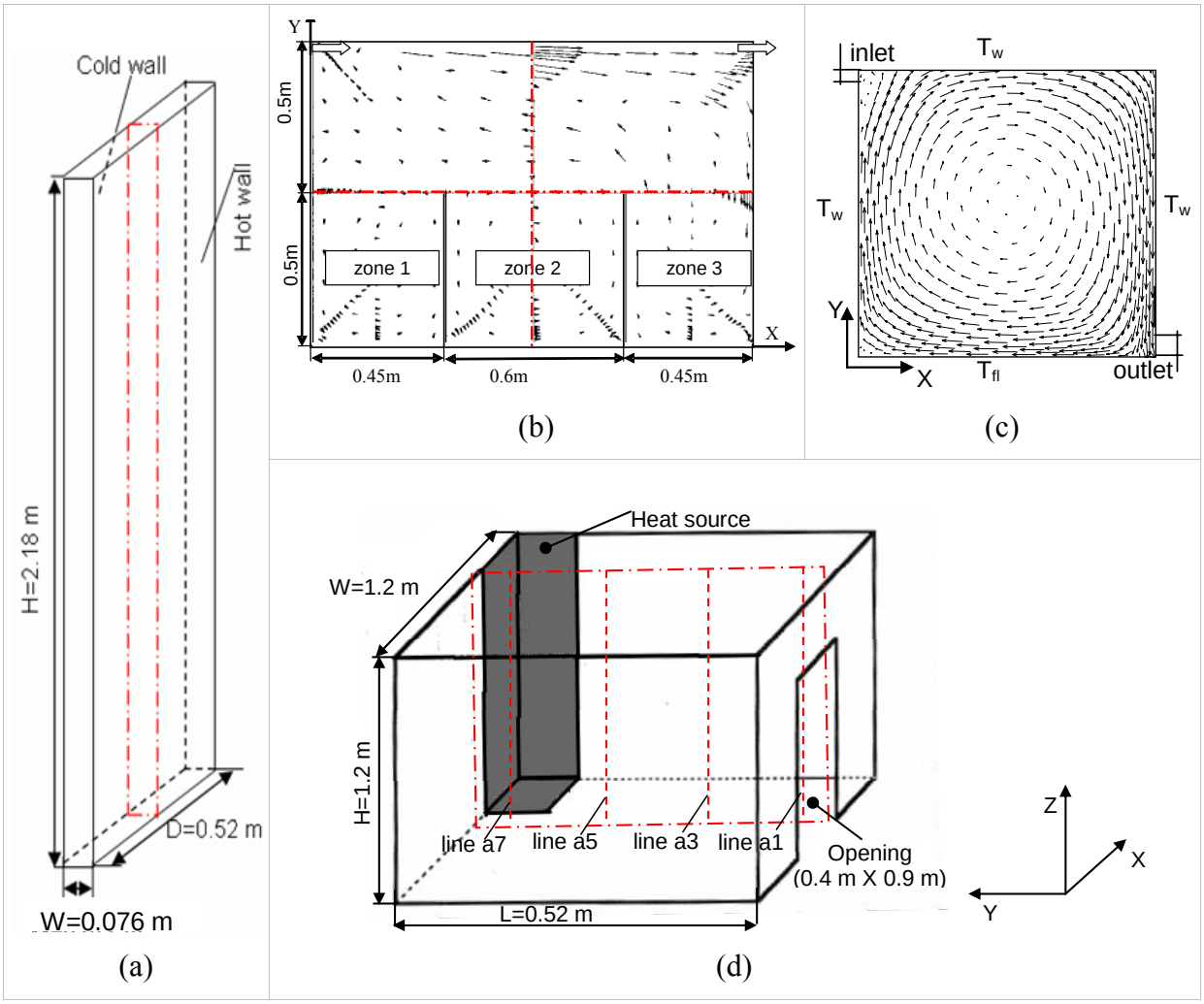

Figure 1. Sketches of the four cases tested: a) natural convection in a tall cavity (Betts and Bokhari, 2000); b) forced convection in a room with partitions (Ito et al., 2000); c) mixed convection in a square cavity (Blay et al., 1992); d) strong buoyant flow in a fire room (Murakami et al., 1995).

Figure 2 compares the simulated results with the measured data. The zero-equation model produced significant errors on the mean air velocity from y/H =0.3 to 0.7 although the predicted air temperature profiles seem acceptable. The LRN-LS model could not predict correctly the air temperature profile near the top and bottom walls. The DES model did not perform well. For velocity prediction, it has similar accuracy compared with the indoor zero equation model. The present DES adopted the S-A one equation model near the walls and the inaccuracy of DES results was mainly associated with the S-A model performance. While the results from the other models reasonably agreed with the experimental data for temperature and vertical velocity, the v2f-dav model exhibited the best agreement.

For the normal Reynolds stress, the v2f-dav and the LES results best agreed with the measurements. The other models only predicted a similar Reynolds stress profile but failed to give the correct magnitudes. The normal component of Reynolds stress $\overline{v'^2}$ can be written as:

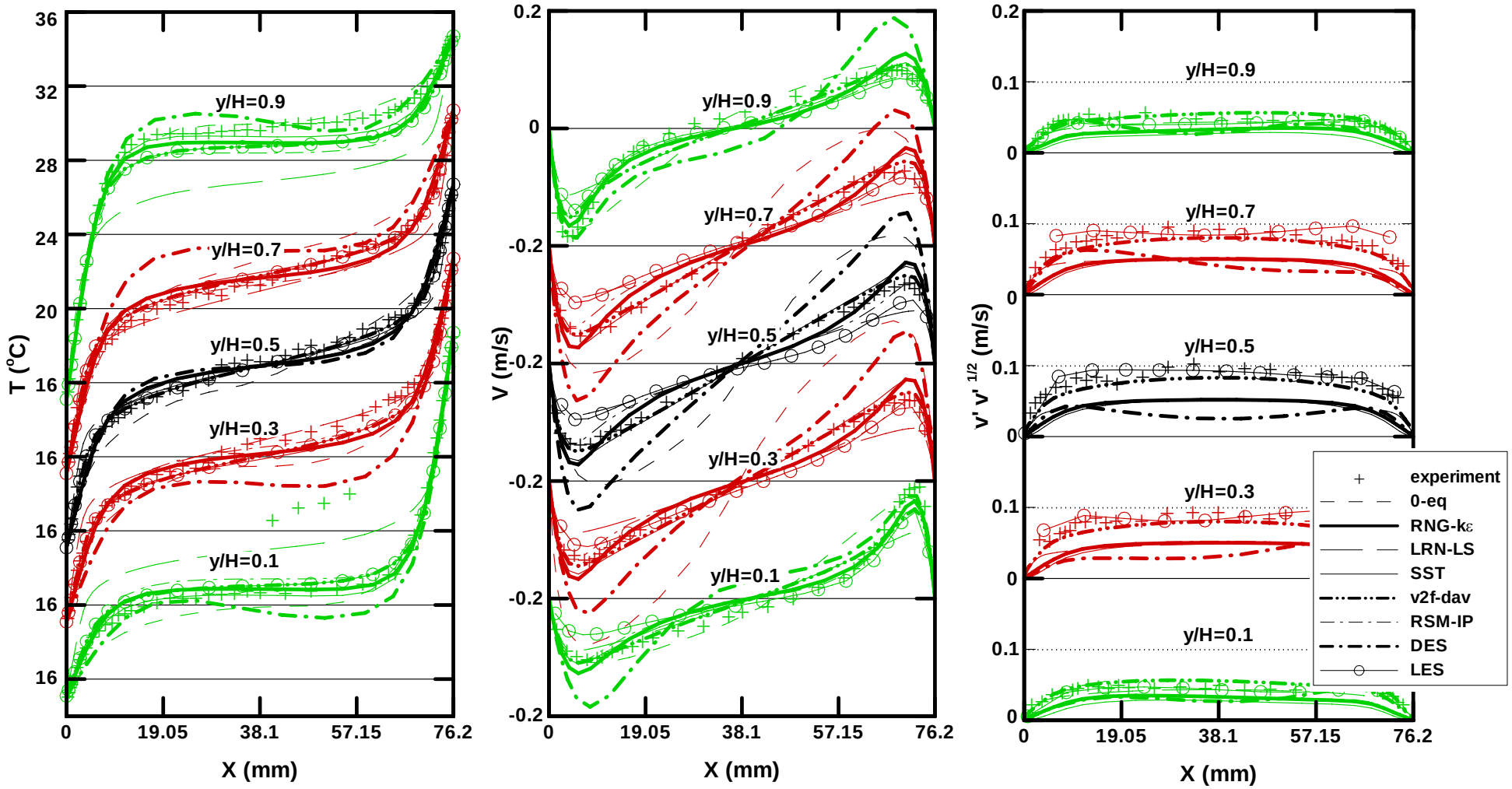

(a) (b) (c)

Figure 2. Comparison of experimental data and numerical simulation for natural convection in the tall cavity: a) air temperature; b) vertical air velocity; c) r.m.s. vertical velocity fluctuation.

$$\overline{v'^2} = \frac{2}{3}\rho k - 2\mu_t \frac{\partial v}{\partial y} \tag{2}$$

The product of the turbulent viscosity and the partial derivative of normal velocity is negligible compared to the turbulence kinetic energy. The under-prediction of $\overline{v'^2}$ for the other models is due to the under-prediction of the turbulence kinetic energy. For all the selected RANS models except the zero-equation model, the k equation has very similar form. The source of the k equation includes three terms: the production, dissipation, and buoyancy production terms. The dissipation term is generally smaller than the production in this case unless very close to wall. The buoyancy production term $G_B = \left(\mu_t / \sigma_{T,t}\right)\frac{g}{\overline{T}}\frac{\partial \overline{T}}{\partial y}$ is about one to two order smaller than that of the turbulence production, which is in the following form:

$$G_k = \mu_t \left\{ 2\left[\left(\frac{\partial u}{\partial x}\right)^2 + \left(\frac{\partial v}{\partial y}\right)^2 \right] + \left(\frac{\partial v}{\partial x} + \frac{\partial u}{\partial y}\right)^2 \right\} \tag{3}$$

Clearly, the $\frac{\partial v}{\partial x}$ is much larger than other partial derivatives in this particular case. Therefore, the inaccurate prediction of $\frac{\partial v}{\partial x}$ influenced the prediction of the turbulence kinetic energy and led to the under-prediction of the normal Reynolds stress. As shown in Figure 2(b), the RNG k-ε model, the LRN model, and the RSM-IP all predicted a lower $\frac{\partial v}{\partial x}$ in the center region of the cavity compared with experimental data. So these models may under predict the overall production of kinetic energy, leading to the inaccuracy of the simulated turbulent stress.

Furthermore, for all the eddy viscosity models the momentum equations have the same form while the only difference is the expression of the eddy viscosity. Except the v2f model the other eddy viscosity models used $\sqrt{k}$ as the velocity scale in determining the eddy viscosity. The inaccuracy on k therefore adversely affected the prediction of mean velocity field and the eddy viscosity. In the present case, the v2f-dav model provided a more suitable eddy viscosity expression and thus achieved a better accuracy.

Forced Convection in a Room with Partitions

Forced convection is often encountered in enclosed spaces with mechanical ventilation systems. Air jets coming out of diffusers and airflow from fans are typical examples of forced convection in rooms. This study used a forced convection case with experimental data from Ito et al. (2000) to analyze the performance of the turbulence models. Figure 1(b) shows the sketch and dimensions of the cross sectional view of the room. The air supply diffuser located at the upper-left corner with a height of 0.02 m in y direction. The exhaust outlet was at the upper-right corner with the same size as the inlet. Two partitions, each 0.5 m high, were located at the lower part of the room.

The room airflow was isothermal and the temperature was about 25ºC. The mean and turbulent velocities were measured by a two-component laser-Doppler velocimeter (LDV). The measured data showed that the mean air velocity did not vary much in the spanwise direction and the

airflow was approximately two dimensional. The mean air supply velocity was 3.0 m/s with a turbulent intensity of 1.6%. The Reynolds number based on the inlet condition was about 4000. Although the room airflow was not laminar, the turbulence level within the domain was very low. Figure 1(b) also shows the measured mean velocity field. The main air stream was attached to the ceiling, and traveled down to zone 3. The main circulation was clockwise. The secondary counter-clockwise circulations were observed in zones 1 and 2.

Figures 3 and 4 show the detailed comparison of the model predictions with the experimental data of velocity and turbulent quantities on the vertical and horizontal center lines labeled as red dash dotted lines in Figure 1(b). All the turbulence models could accurately predict the air jet flow pattern near the ceiling. For the prediction of various circulations in the room, the model performance varies. The indoor zero-equation model predicted a reversed U velocity profile in zone 2 as shown in Figure 4. Similarly, the SST k-ω model predicted a reversed V velocity profile in zone 1 indicating a wrong air circulation pattern. Meanwhile, the SST k-ω model produced the least satisfactory agreement with the experimental data compared to the other models. In principle, the SST k-ω model should have similar performance as the k-ε model in regions far away from the walls. The blending function F_1 in Table 1 was designed to automatically switch to the k-ε model formulation outside the boundary layers where F_1 should vanish. Figure 5 shows the computed value of F_1 in the domain. The F_1 value was large even far away from the walls. So the SST k-ω model essentially worked as a k-ω model rather than a k-ε model in this case. In fact, the SST k-ω model uses limiting functions to ensure blending functions vanished outside the wall region (Menter, 1994). Those limiting functions have been tested to be valid for many turbulent flows. Nevertheless, the turbulence level in room air is generally very low and those limiting functions may not be always valid. It is necessary to modify the blending functions in order to improve the accuracy of the SST k-ω model in such low-turbulence airflow. The DES model under predicted the vertical velocity fluctuation and resolved Reynolds stress as shown in Figure 3. Again, the errors may come from the RANS form of the DES model although no clear evidence can be provided at present. Further investigation on this and other DES models may improve our understanding of the inherent problem. Besides the zero equation and the SST k-ω models, the other models have similar accuracy although some small disparities exist.

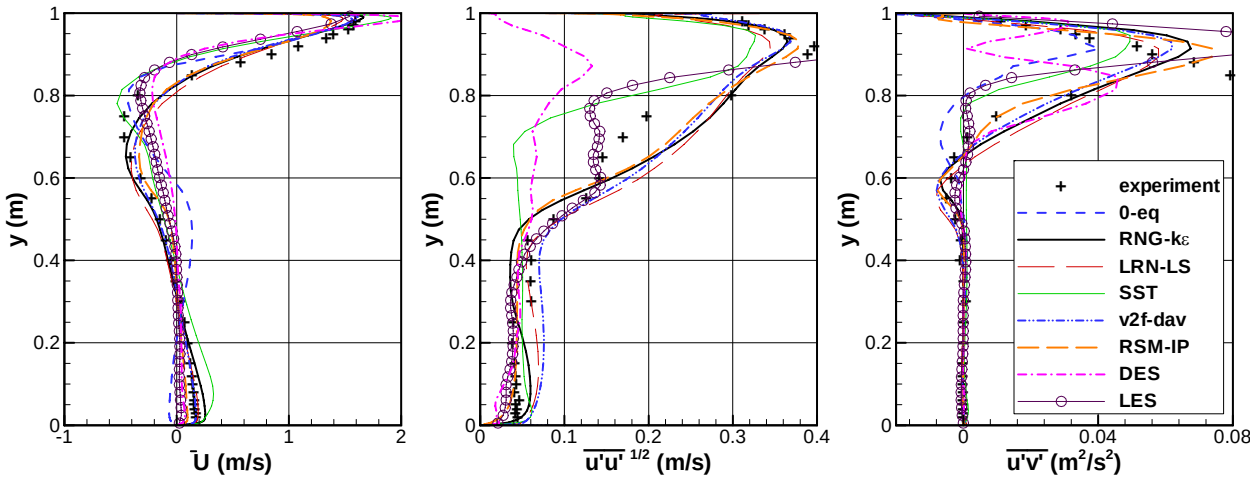

Figure 3. Comparison of the numerical results with the experimental data along the vertical centerline in the room with forced convection.

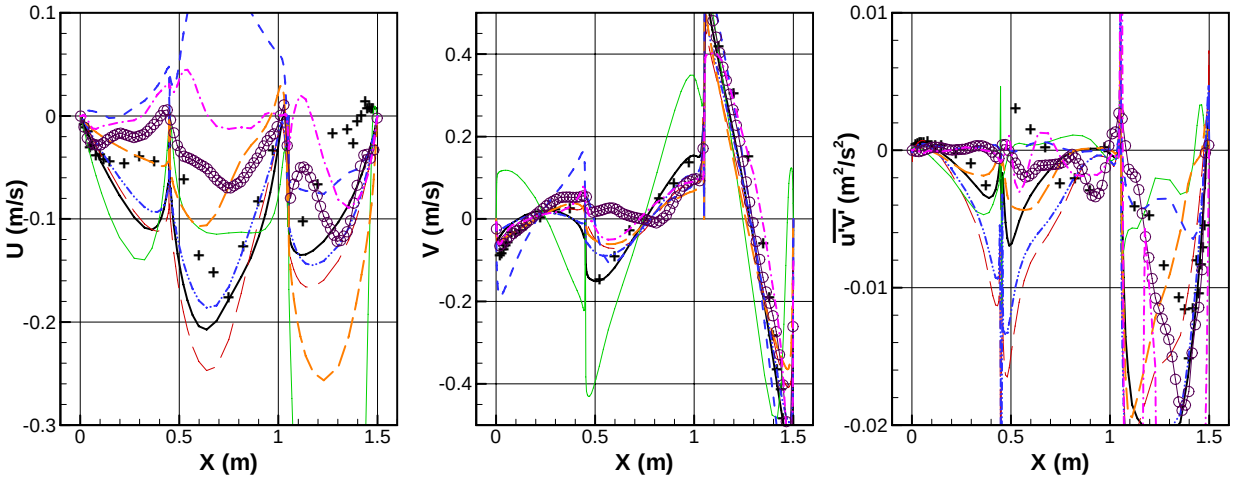

Figure 4. Comparison of the numerical results with the experimental data along the horizontal centerline in the room with forced convection. (Curves represent the same models as in Figure 3.)

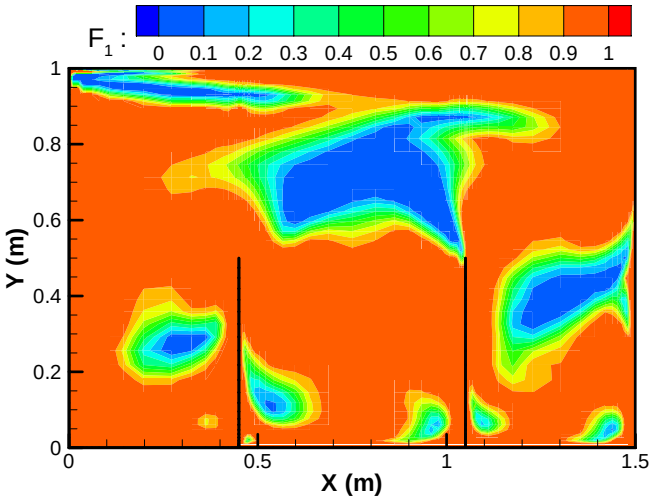

Figure 5. The computed blending function F_1 of the SST k-ω model in the forced convection case.

Mixed Convection in a Square Cavity

Mixed convection is the most common airflow form in an air-conditioned environment. Blay et al. (1992) studied a mixed convection flow in a square cavity using both experimental and computational methods. Shown in Figure 1(c), air was discharged from the inlet slot at the ceiling level and exhausted at the floor level on the opposite wall, and the floor was heated. The measured inlet conditions were: $u_{in} = 0.57$ m/s; $v_{in} = 0$; $T_{in} = 15$ºC; $\varepsilon_{in} = 0$; and $k_{in} = 1.25\times10^{-3}$ m^2/s^2. The wall temperature T_w was 15ºC and the floor temperature T_{fl} was 35.5ºC. The Reynolds number based on the inlet condition was 684.

All the RANS models were simulated two-dimensionally. With a grid resolution of 60×60 in the two-dimensional domain the y^+ for the first grid was about 1. For LES and DES 30 uniform

grids were placed in the spanwise direction while the grid resolution in cross section was the same as that for RANS. Figure 6 presents the numerical results.

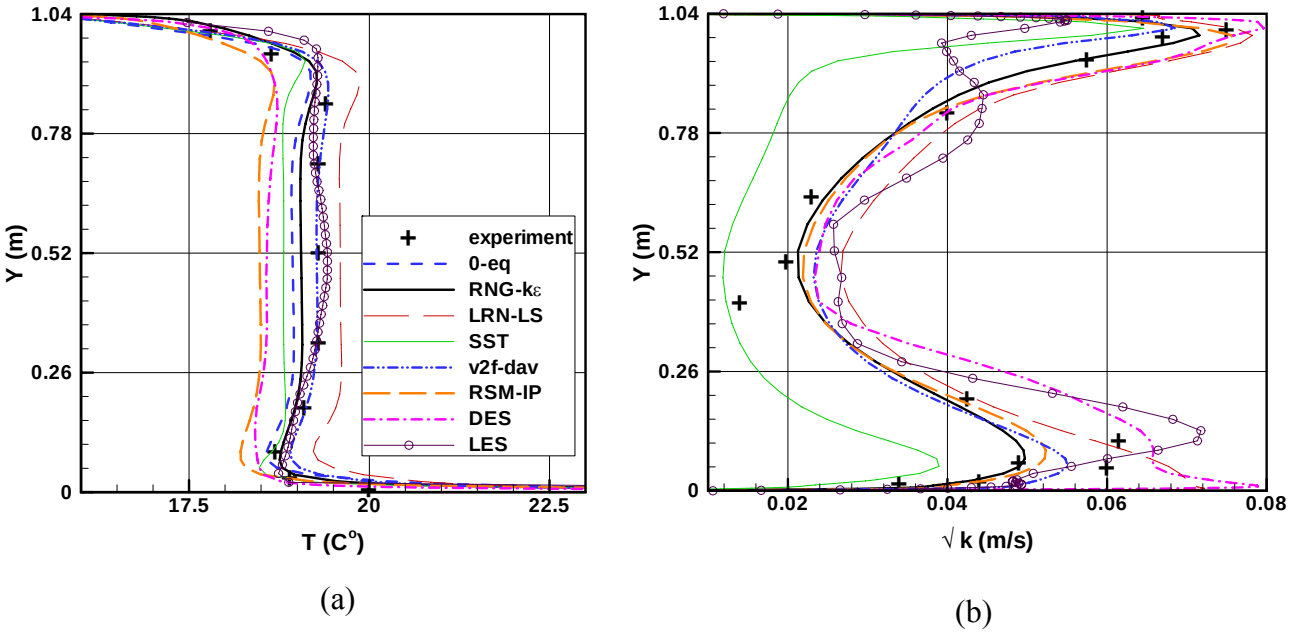

(a) (b)

Figure 6. Comparison of simulated and measured results on the centerline X/L = 0.5 in the room with mixed convection: a) temperature; b) turbulence kinetic energy.

In general all the numerical simulations agreed reasonably with the experimental data for the air temperature profile. For the temperature prediction, the LES and the v2f-dav agreed better with the measured data than the other models. Most of the models can also calculate the turbulence kinetic energy fairly well except the SST k-ω model. Overall, the SST model predicted the turbulence kinetic energy 50% lower than the measurement while this result was similar to that by a standard k-ω model (the results not shown here). As discussed in the forced convection case, the SST model might not switch to k-ε model in regions far from the walls when the flow turbulence level is relatively low. Special care must be taken to apply the SST model in such flow regime while some modifications on the model blending functions may be needed.

Strong Natural Convection in a Model Fire Room

The three cases studied above represent the typical flow mechanisms in enclosed environments. Some models performed reasonably well for both cases while the others not. Another case with extreme buoyancy conditions was employed to test further the robustness of those models in a more challenging scenario: a model fire room with strong buoyancy flow. This case was designed by Murakami et al. (1995) who measured detailed mean and turbulence quantities. The chamber dimensions were 1.8 m long by 1.2 m wide by 1.2 m high as shown in Figure 1(d). The total heat power input from the heat sources was 9.1 kW with an average surface temperature higher than 500 ºC. The opening size was 0.4 m wide by 0.9 m high. The air flowed through the opening between the chamber and its outside enclosure. The outer enclosure was of a size about 8000 m^3. All the walls of the chamber were well insulated. Velocity vectors were measured by a two-component LDV. The air and wall temperatures were measured by thermocouples.

For the numerical simulations, this study included a part of the outside enclosure into the computation domain. The inclusion can avoid the numerical instability by setting pressure boundary condition for the opening of the model room. So the opening can be treated as an interior one. In order to save computing time, the grids in the included outside enclosure were rather coarse. But the grids inside the chamber remained reasonably fine (70 (L) × 55 (W) × 60 (H) =231,000 cells) with an averaged $y^+ = 1$ for the first grids near to the walls. In numerical simulation, the outer enclosure size was set to 10m (X) × 20 m (Y) × 5m (Z). Including the grids for the outer enclosure, the total grid number was 350,000. Since the grid in the enclosure is too coarse for a LES, the LES did not include the outside enclosure part.

Inside the chamber, the temperature difference can be on the order of several hundred of Kelvin. The large temperature gradient caused significant air density change while the flow was still incompressible (low Ma number). Thus the density variation needs to be considered by using the ideal gas law, rather than the Boussinesq approximation,

$$\rho = \frac{p_{op}}{RT} \tag{4}$$

where p_{op} is the operating pressure in the room (here 1atm at sea level), R the gas constant and T the air temperature.

The comparison between the numerical and experimental results in four measurement locations is shown in Figure 7. The RSM model could not converge with the grid distribution and boundary conditions used. This is likely due to the coarse grid used in the outer space. Thus its results are not presented in the figure. For the mean temperature and velocity, all the predictions presented agreed reasonably well with the measured data. Note that the buoyancy production term was added into the v2f-dav model. Due to the strong buoyancy effect in the chamber, the buoyancy production term is not negligible in the source terms of the turbulent kinetic energy equation.

Generally, all the models gave a very good prediction of the mean temperature and velocity. The models, however, have obviously different performance on predicting the velocity fluctuation. The RNG k-ε model under-predicted the fluctuating velocity in the lower part of the room. By examining Equation (2) for the expression of $\overline{v'^2}$, the ρk term, in this case, is at least one order of magnitude larger than the other on the right hand side of Equation (2). Similar to the natural convection case in the tall cavity, the under-prediction of $\overline{v'^2}$ is likely due to the under-prediction of k. The v2f and the RNG k-ε model have the exact same form of the k equation except the expression of eddy viscosity while the v2f-dav model has better accuracy. Thus the inaccurate $\overline{v'^2}$ prediction is possibly associated with the eddy viscosity formulation of the k-ε model as well as the near wall treatment. In addition to the v2f-dav model, the SST k-ω and LRN models also have much better performance than the high Reynolds number k-ε model. The SST model could successfully switch between the k-ω and k-ε models as the airflow in the model room is more turbulent compared with the previous two cases. The near wall treatment of a k-ω formulation worked better than that of a high Reynolds number k-ε model in this case. The present low Reynolds modification (Launder and Sharma, 1974) worked also reasonably well and did improve the performance of high Reynolds number k-ε models.

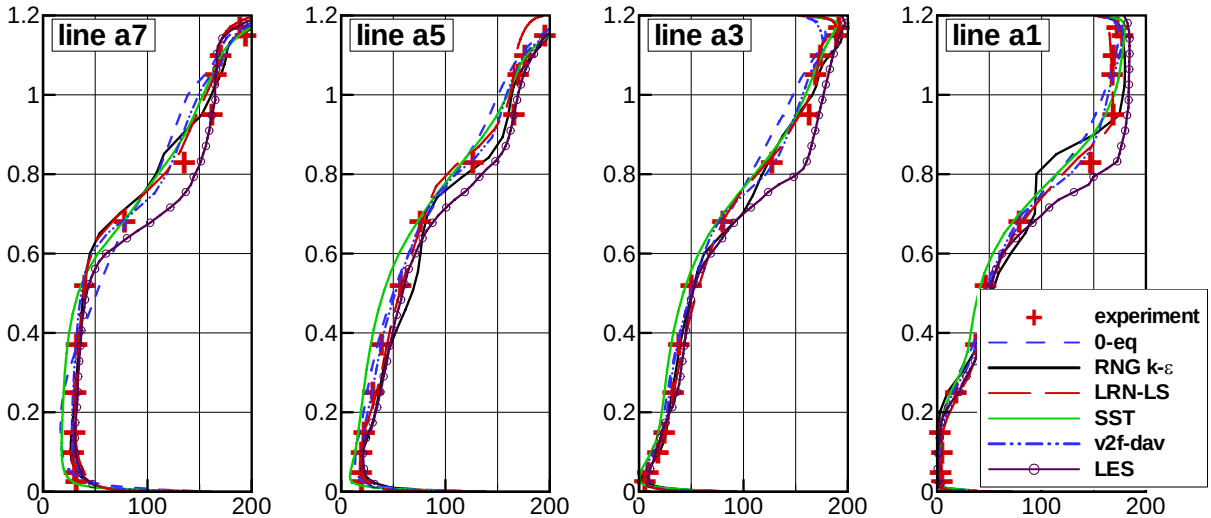

(a) $T-T_\infty$ (°C)

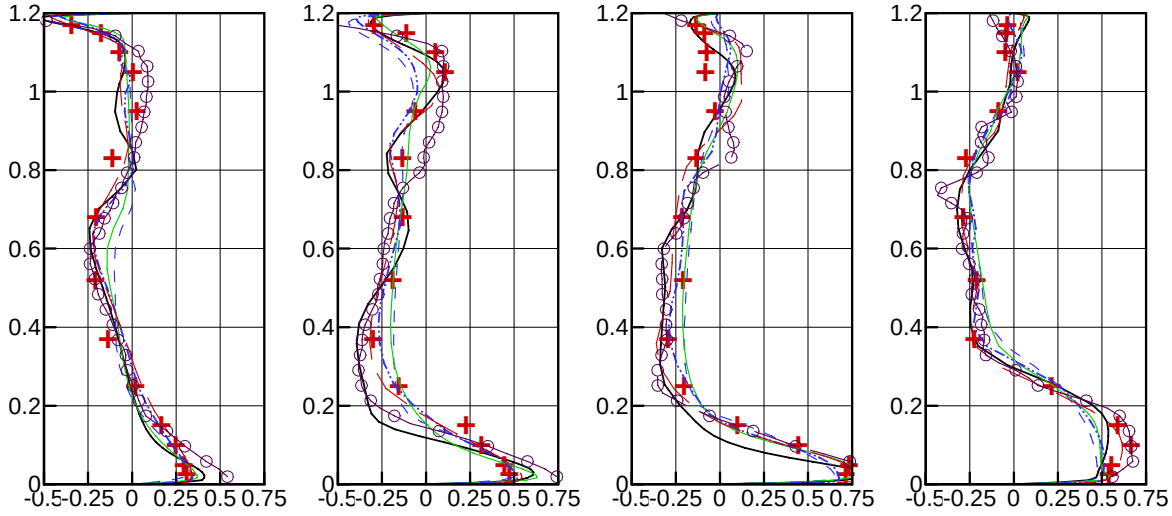

(b) V (m/s)

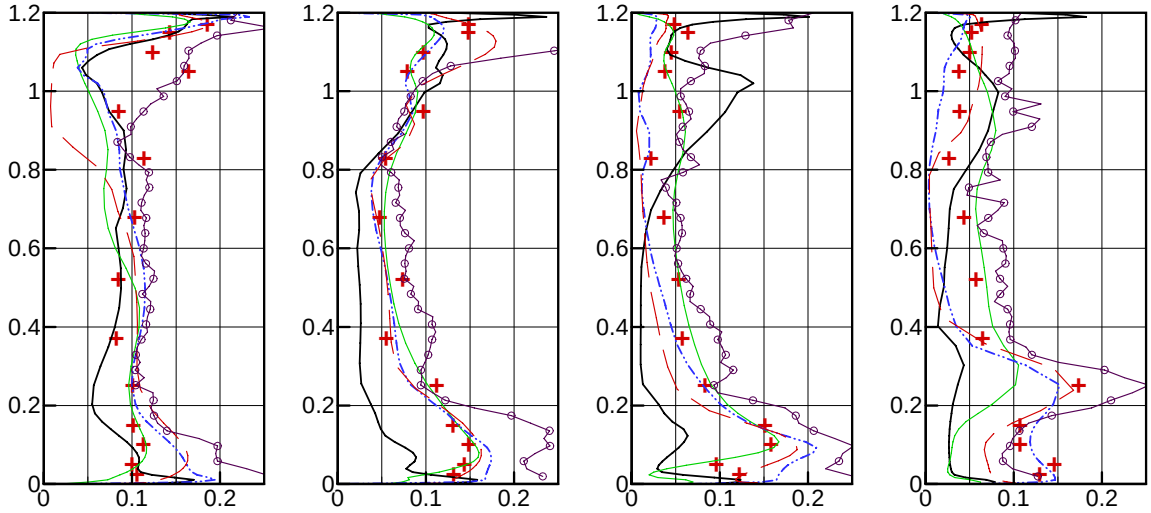

(c) $\overline{v'^2}$ (m/s)

Figure 7. Comparison of simulated and measured results on four measurement locations: a) temperature; b) horizontal velocity; c) normal turbulent stress in horizontal direction

The LES results agreed with the measurement well in the center of the room but were less accurate near the wall. The errors near the walls are likely due to the limited ability of the subgrid scale model used here (Lilly, 1992). The SGS model is essentially algebraic model for subgrid scale eddies. The algebraic nature of the SGS model affects the LES accuracy close to the wall especially when the turbulence is not locally in equilibrium. Therefore, the LES could be less accurate than some of the eddy viscosity models.

The accuracy of the zero-equation model in this case was remarkable. Its results are comparable to those more advanced models. In addition, the zero-equation model was fastest and most stable. In fact, the other RANS models tested used the flow and temperature field calculated by the zero-equation model as initial conditions. Otherwise, the convergence of some models would be very difficult or even impossible.

DISCUSSION

The model accuracy has been analyzed by comparing their predicted results with the experiment data. Besides the accuracy, the computing cost is another important aspect that relates to the model performance.

All the RANS and DES simulations for the first three cases were conducted on a personal computer with Pentium IV, 3.0 GHz CPU with 1G memory. The RANS simulations for the fourth case were conducted in a computer cluster of three dual-CPU nodes with 2G Hz CPU speed and 3.7 GB memory for each node. All the LES simulations (except the fourth case) were performed on a compute cluster with 4 nodes and each node has a AMD Opteron (64-bit), 2.6GHz CPU with 1G memory. Generally four factors influence the computing time: (1) the grid resolution, (2) the discretization scheme, (3) the degree of non-linearity of the model, and (4) the number of PDEs the model contains. By fixing the first two factors, the difference of computing time is the mainly attributed to the turbulence model itself. Taking the 2D mixed convection case for example, all simulations were based on the same grid resolution (60×60). The indoor zero-equation model required 2 minutes of computing time, the RNG k-ε model 7 minutes, SST k-ω model 8 minutes, the v2f-dav model around 13 minutes, the LRN-LS 15 minutes, and the RSM-IP 35 minutes, respectively. The DES used 14-day computing time to finish the calculation of 20000 time steps with each time step of 0.01 s. The LES used 8 days to finish the transient calculation on the cluster.

Table 2 summarizes the relative computing time along with the model accuracy as discussed. In general, the RNG k-ε and SST k-ω models required roughly 2-4 times as long computing time as the indoor zero equation model, while the v2f-dav model and the LRN model required 4-8 times as long as the 0-eq. model. The RSM model required the most computing time among all RANS models tested. But the convergence of the RSM model is not as satisfactory as others. Compared with RANS, the computing effort of LES is significantly longer. With the computer clusters, the LES could handle some indoor airflows with simple domains. However, it can be still prohibitively time consuming to use LES for very complicated enclosed environments. The DES required similar computing time as of LES based on the same grid. By carefully designing the grid resolution, the DES could save more computing time from pure LES although the overall computing time required is still very high.

It is necessary to quantify the model accuracy criteria A, B, C, and D in Table 2. Due to the complexity, a strictly quantified and objective description is difficult. In general, this study used the relative error between prediction and measurement at measured points as a major criterion. If

this error is less than 10% or larger than 50% at most measured points, the model accuracy is rated as A or D, respectively. While ratings A and D quantify the extremes the difference between B and C can be more subtle. Rating B is given to predictions with relative error less than 20-30% at most measured points. Rating C is given to the remaining predictions. Note that the relative error calculations for the temperature were based on the nominal temperature differential, which has different definition for each case. In the natural convection case, the nominal temperature difference is the wall temperature difference between the hot and the cold walls. For the mixed convection case, it is defined as the difference between the inlet and the outlet temperatures. For the strong buoyancy flow case, it is the difference between the measured local temperature and the environment temperature.

Table 2. Summary of the Performance of the Turbulence Models Tested by This Study.

Cases	Compared items	Turbulence models							
		0-eq.	RNG k-ε	SST k-ω	LRN -LS	V2f-dav	RSM-IP	DES	LES
Natural convection	Mean Temp.	B	A	A	C	A	A	C	A
	Mean Velo.	D	B	A	B	A	B	D	B
	Turbulence	n/a	C	C	C	A	C	C	A
Forced convection	Mean Velo.	C	A	C	A	A	B	C	A
	Turbulence	n/a	B	C	B	B	B	C	B
Mixed convection	Mean Temp.	A	A	A	A	A	B	B	A
	Mean Velo.	A	B	B	B	A	A	B	B
	Turbulence	n/a	A	D	B	A	A	B	B
Strong buoyancy flow	Mean Temp.	A	A	A	A	A	n/c	n/a	B
	Mean Velo.	B	A	A	A	A	n/c	n/a	A
	Turbulence	n/a	C	A	B	B	n/c	n/a	B
Computing time (unit)		1	2 - 4		4 - 8		10 - 20	10^2 - 10^3	

A = good, B = acceptable, C = marginal, D = poor, n/a = not applicable, n/c = not converged.

CONCLUSIONS

This study evaluated the overall performance of eight prevalent and/or recently proposed models for modeling airflows in enclosed environments. Four benchmark indoor flow cases were tested that represent the common flow regimes in enclosed environments. In general, the LES provide the most detailed flow features while the computing time is much higher than the RANS models and the accuracy may not always be the highest. The DES also required significant computing time in typical indoor flows. For these low-Reynolds-number flows, the DES does not save computing time while the accuracy becomes poorer compared with the LES with the same grid. More investigations are needed to draw conclusive remark on using DES for airflow simulations of enclosed environments.

Among the RANS models, the v2f-dav and RNG k-ε models have the best overall performance compared to the other models in terms of accuracy, computing efficiency, and robustness. Both models are recommended for indoor airflow simulations. Although the present investigation has evaluated the selected turbulence models for four common scenarios, other important flow

scenarios (e.g. three dimensional wall jets in ventilated rooms and wind driven natural convection flows) should be further investigated.

The SST k-ω model did improve the accuracy in strong buoyant flow scenario without significantly increasing computing time compared with the RNG k-ε model. However, the SST k-ω model has exhibited problems for low turbulence flows. The LRN-LS model and the v2f-dav model require similar computing time, but the LRN-LS model did not perform as well as the other. The RSM model performed reasonably well in the two-dimensional flows, but encountered convergence problem in the three-dimensional buoyant flow.

Compared with these advanced turbulence models, the indoor zero equation model is less accurate. Nevertheless, the model also has its merits. It is simple and always has good convergence speed. Its results can be used as good initial fields for more advanced models to achieve converged results.

While the turbulence models have different performance in different flow categories, each airflow category favors specific turbulence models. The present study therefore summarizes the best suited turbulence models for each flow category studied. The v2f-dav and the LES are best suited for the low Rayleigh number natural convection flow in predicting air velocity, temperature and the turbulence quantities. In the forced convection flow with low turbulence levels, the RNG k-ε, the LRN-LS, the v2f-dav, and the LES all performed very well. The v2f-dav, the RNG k-ε, and the indoor zero equation model have the best accuracy and are suitable for mixed convection flows with low turbulence levels. Although the SST k-ω model is less accurate than other models in low Reynolds number flows, it works the best in the high Rayleigh number buoyancy driven flow. Meanwhile, the LRN-LS and the v2f-dav model are also suitable for the high Rayleigh number flow in the present study.

NOMANCLATURE

Symbols

C	concentration of scalar variables; constants and coefficients in Table 1	k	turbulent kinetic energy
c_p	specific heat capacity at constant pressure	Re	Reynolds number
D	the LRN modification term in the k-equation of the standard k-ε model	S	source terms in the transport equations; magnitude of strain rate tensor
E	the LRN modification term in the ε-equation of the standard k-ε model	T	air temperature or turbulence time scale
F	weighting function in SST k-ω model	t	time
f	the damping function for the LRN model or the elliptical relaxation in the v2f model	u	instantaneous air velocity
G	the production term in various transport equations	$\overline{v'^2}$	root mean square of fluctuating velocity normal to wall
H	enthalpy	x	Cartesian coordinates
h	subgrid Scale turbulent heat flux in LES	Y	dissipation term in various transport equations

Greek symbols

Δ	filter width of filter function in LES in Table 3.1	μ_τ	turbulent viscosity of fluid flow
ε	the dissipation rate of turbulence kinetic energy	ρ	air density
ϕ	the symbol of general variable in equation (1) and Table 1	$\sigma_{\phi,t}$	turbulent Prandtl numbers of variable ϕ
Γ	diffusion coefficient in equation (1)	τ	stress
κ	von Karman constant (=0.4187)	Ω	magnitude of rotation tensor
μ	molecular viscosity of a fluid	ω	rate of dissipation per unit turbulent kinetic energy

Super Scripts

s	subgrid scale variables in LES	'	fluctuating quantities

Sub Scripts

i, j, l, m	Cartesian coordinates

ACKNOWLEDGEMENT

The authors would like to express their gratitude to Dr. Kazuhide Ito of Tokyo Polytechnic University who kindly provided the details of his experimental data of the natural convection case. Z. Zhang and Q. Chen would like to acknowledge the financial support to the study presented in this paper by the U.S. Federal Aviation Administration (FAA) Office of Aerospace Medicine through the Air Transportation Center of Excellence for Airliner Cabin Environment Research under Cooperative Agreement 04-C-ACE-PU. Although the FAA has sponsored this project, it neither endorses nor rejects the findings of this research. The presentation of this information is in the interest of invoking technical community comment on the results and conclusions of the research.

REFERENCES

Betts, P.L., and I.H. Bokhari. 2000. Experiments on turbulent natural convection in an enclosed tall cavity. *Int. J. Heat & Fluid Flow* 21:675-683.

Blay, D., S. Mergur, and C. Niculae. 1992. Confined turbulent mixed convection in the presence of a horizontal buoyant wall jet. *Fundamentals of Mixed Convection*, ASME HTD 213:65-72.

Chen, Q., and W. Xu. 1998. A zero-equation turbulence model for indoor airflow simulation. *Energy and Buildings* 28(2):137-144.

Davidson, L., P.V. Nielsen, and A. Sveningsson. 2003. Modification of the V2F model for computing the flow in a 3d wall jet. *Turbulence Heat and Mass Transfer* 4:577-584.

Fluent. 2005, *Fluent 6.2 Documentation*, Fluent Inc., Lebanon, NH.

Germano, M., P. Piomelli, P. Moin, and W.H. Cabot. 1991. A dynamic subgrid-scale eddy viscosity model. *Physics of Fluids* 3(7):1760-1765.

Gibson, M. M., and B.E. Launder. 1978. Ground effects on pressure fluctuations in the atmospheric boundary layer. *J. Fluid Mech.* 86:491-511.

Ito, K., S. Kato, and S. Murakami. 2000. Model experiment of flow and temperature field in room for validating numerical simulation analysis of newly proposed ventilation effectiveness. *J. Archit. Plann. Environ. Eng. (In Japanese)* 534:49-56.

Launder, B.E., and B.L. Sharma. 1974. Application of theenergy dissipation model of turbulence to the calculation of flow near a spinning disk. *Letters in Heat Mass Transfer*(1):131-138.

Lien, F., and G. Kalitzin. 2001. Computations of transonic flow with the v2−f turbulence model. *Int. J. Heat Fluid Flow* 22:53–61.

Lilly, D.K. 1992. A proposed modification of the Germano subgrid-scale closure model. *Physics of Fluids* 4:633-635.

Menter, F.R. 1994. Two-equation eddy-viscosity turbulence models for engineering applications. *J. AIAA* 32:1598-1605.

Murakami, S., S. Kato, and R. Yoshie. 1995. Measurement of turbulence statistics in a model fire room by LDV. *ASHRAE Transactions* 101:3905.

Shur, M., P.R. Spalart, M. Strelets, and A. Travin. 1999. Detached-eddy simulation of an airfoil at high angle of attack. *In 4th Int. Symposium on Eng. Turb. Modeling and Experiments*. Corsica, France, May.

Spalart, P., and S. Allmaras. 1992. A one-equation turbulence model for aerodynamic flows. Technical Report AIAA-92-0439.

Yakhot, V., and S.A. Orszag. 1986. Renormalization group analysis of turbulence. *Journal of Scientific Computing* (1):3-51.

Zhai, J. Z., Z. Zhang, W. Zhang, and Q. Chen. 2007. Evaluation of Various Turbulence Models in Predicting Airflow and Turbulence in Enclosed Environments by CFD: Part-1: Summary of Prevalent Turbulence Models. *ASHRAE HVAC&R Research* (accepted).